



# Analysis of thrust force and delamination in drilling GFRP composites with candle stick drills

Liping Liu<sup>1</sup> · Chunliang Qi<sup>1</sup> · Feng Wu<sup>1</sup> · Xiaofeng Zhang<sup>2</sup> · Xueming Zhu<sup>3</sup>

Received: 28 June 2017 / Accepted: 10 November 2017 / Published online: 25 November 2017  
© Springer-Verlag London Ltd., part of Springer Nature 2017

## Abstract

Drilling is an indispensable process for assembling the composites components. The drilling-induced delamination damage generally refers to the peel up delamination on the entrance surface and the push down delamination on the exit surface. Many researchers have carried out studies on drilling force and delamination damage in composites using special drills. Candle stick drills have been recognized as advantageous tools for the reduction of thrust force and delamination damage in drilling composites. Drilling experiments of glass fiber-reinforced plastic (GFRP) composites and finite element simulations were carried out in this paper. Three candle stick drills with different drill tip geometries and one twist drill were compared in terms of thrust force, peel up delamination, and push down delamination. The results revealed that, compared to twist drill, not all candle stick drills could get relatively good drilling results. What is more, drilling results of candle stick drills had a great relationship with the drill tips geometry angles. Finally, an optimized candle stick drill with appropriate drill tip geometry achieved relatively excellent drilling results.

**Keywords** Drilling · GFRP · Thrust force · Delamination · Candle stick drill

## 1 Introduction

The glass fiber-reinforced plastic (GFRP) composites have been widely used in various industries in recent years due to their excellent properties, such as light weight, high modulus, high specific strength, and good corrosive resistance. Drilling is frequently used in assembling composites components due to the need of the fastener mechanical connection. The drilling of GFRP composites due to their heterogeneity, anisotropy, and abrasion resistance is quite different from that of ordinary metals and their alloys and is often accompanied with multiple damages, such as tool wear, rough surface finish, burr, tearing, fiber pull-out, thermal damage, matrix crack, and delamination. The most serious damage is surely delamination that can

happen both at the entrance and exit of the laminate, and generally refers to the peel up delamination at the entrance surface and push down delamination at the exit surface [1–4].

A large number of researches have carried out corresponding studies on drilling composites using traditional twist drill. Palanikumar et al. [5] conducted drilling experiments in composites to study the influence of the machining parameters on push down delamination. They revealed that feed speed was the main factor which had the greatest influence on push down delamination, followed by rotational speed. The study conducted by Latha and Senthilkumar [6] revealed that feed rate and drill diameter were the main factors which impacted the push down delamination in drilling of GFRP composites. The spindle speed showed only limited effect on push down delamination in drilling of GFRP composites. The study conducted by Kilickap et al. [7, 8] revealed that the peel up delamination and the push down delamination increased with the increase of feed rate and cutting speed in drilling of composites. Won and Dharan [9] indicated that push down delamination had a great relationship with the thrust force, and most of the thrust force was generated by the chisel edge. So, increasing the length of the chisel edge resulted in an increasing in thrust force and consequently, the risk of push down delamination. So, changing the drill bit geometry might have a

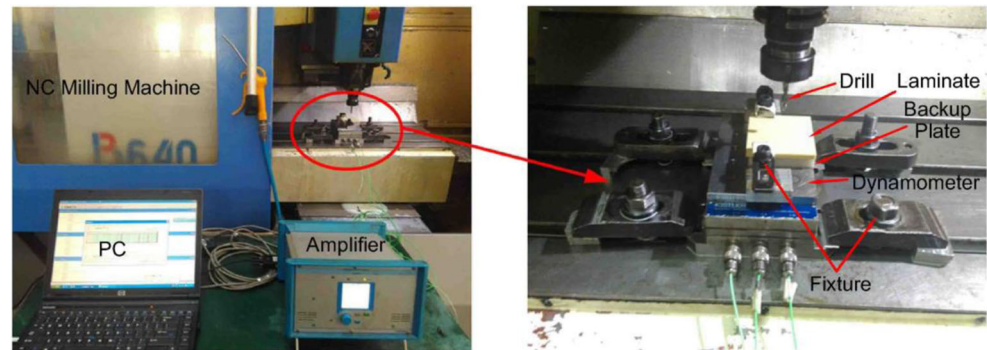
✉ Liping Liu  
liuliping\_tj@163.com

<sup>1</sup> School of Aerospace Engineering, Civil Aviation University of China, Tianjin 300300, China

<sup>2</sup> School of Mechanical Engineering, Tianjin University, Tianjin 300350, China

<sup>3</sup> School of Mechanical Engineering, Tianjin University of Technology and Education, Tianjin 300222, China

Fig. 1 Experimental platform



significant impact on the thrust force and corresponding delamination damage. The comprehensive modeling and analysis of special drill bits [10], including saw drill, candle stick drill, core drill, core-saw drill and step drill, illustrated that a distributed thrust toward the drill periphery rather than concentrated at hole center (twist drill) was advantageous. Tsao [11] experimentally investigated the trust force of core drill with drill parameters (grit size of diamond, thickness, feed rate and spindle speed) in drilling CFRP. Then, in the investigations from Tsao [12], thrust force and delamination by core-saw drill during drilling CFRP were selected as quality character factors to optimize drilling parameters (diameter, feed rate, and spindle speed). What is more, the thrust force of step drill with drilling parameters (step angle, stage ratio, feed rate, and spindle speed) in drilling CFRP is experimentally investigated by Tsao [13].



Fig. 2 UNION optical microscope

Tsao et al. [14, 15] had explained that the saw drill and candle stick drills had a smaller center than twist drill. So, the saw drill and candle stick drills could be operated at larger feed rate without push down delamination damage compared to the twist drill. That is, the saw drill and candle stick drills offered the higher critical thrust force causing the onset of delamination than the twist drill. At the same time, in the actual drilling process, an eccentric candle stick could degrade the quality of the fiber-reinforced material, and the critical thrust force that will produce delamination decreased with increasing the eccentricity [16]. Palanikumar et al. [17–20] analyzed in detail the influences of machining parameters on thrust force and delamination in drilling GFRP using candle stick drills. Experimental results showed that the drilling performance in composites could be improved by optimizing the drilling parameters. In the process of optimizing drilling parameters, Grilo et al. [21] evaluated the machinability of drilling CFRP using the candle stick drill. The results indicated that the candle stick drill allowed drilling composites with no delamination in both sides of hole at the best drilling parameters. Wang et al. [22] also evaluated the machinability of drilling CFRP using the candle stick drill. But the results indicated that candle stick drill would induce the unexpected delamination even at its best drilling parameters. Abrão et al. [23, 24] investigated the effect of cutting tool geometry on thrust force and push down delamination in drilling of glass fiber-reinforced composite. The candle stick drills achieved lower thrust force and push down delamination than the twist drill. Its geometry allowed the cutting action to happen from the outer to the inner tool diameter, similarly to a trepanning

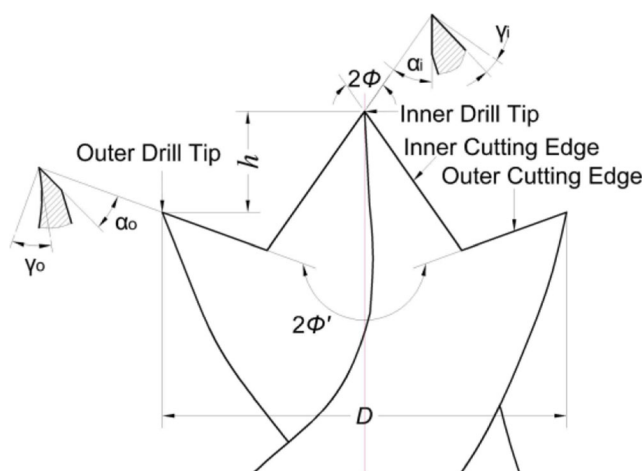
Table 1 Glass fiber-reinforced plastic

Parameters	Values
Laying	$0^\circ [-45^\circ 90^\circ 45^\circ \bar{0}^\circ]_{3S} 0^\circ$
Fiber density	$2.5 \text{ g/cm}^3$
Fiber volume fraction	54%
Thickness	5.25 mm

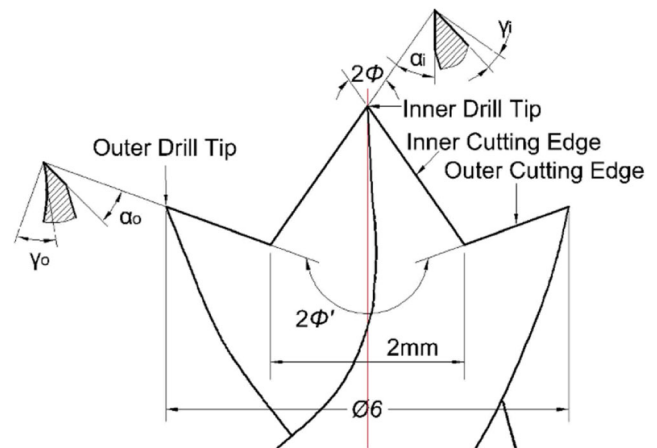
**Table 2** Glass fiber-reinforced plastic performance parameters

Parameters	Values
Strength of extension	550 Mpa
Modulus of extension	28 Gpa
Flexure strength	630 Mpa
Flexure modulus	30 Gpa
Compression strength	300 Mpa

tool. Tan et al. [25–27] studied the influence of drill geometry on thrust force and delamination in drilling of composite materials using different drill bits. The results indicated that candle stick drills obtained the higher level of thrust force, peel up, and push down delamination than the twist drill. The candle stick drills used in the above studies were not exactly same in the drill tip geometry structure. So, it could be inferred from above studies that, compared to the twist drill, not all candle stick drills could get relatively good drilling quality. It could also be inferred from these results that the geometric angles of the candle stick drill tips might have a significant impact on the drilling quality. Chen et al. [28, 29] studied the effect of point angle and helix angle on thrust force. They uncovered that the thrust force increased with the increase in the point angle, and the thrust force decreased with the increase in the helix angle. Piquet et al. [30] experimentally analyzed the drilling damage in thin carbon/epoxy plate using special drills. The experimental results have shown that the rake angle of cutting edges had an important impact on the peel up delamination. Faraz et al. [31, 32] analyzed the influence of the rake angle of cutting edge and point angle on thrust force, peel up delamination, and push down delamination. They revealed that the thrust force increased with the increase in point angle, the peel up delamination reduced with the increase in point angle, and peel up, and push down delamination increased with the increase in rake angle of cutting edge. The above researches on the geometric angles of the drill tip were mainly



**Fig. 3** Special geometry of candle stick drill



**Fig. 4** Geometry of three candle stick drills

focused on twist drills or between different types of drill bits, but no compressive study about the impact of the geometric angles of candle stick drill tips on drilling process.

In this work, three candle stick drills with distinct drill tip geometries and one twist drill were applied in drilling GFRP laminates. The influences of the specific geometric angles of drill tip on thrust force, peel up, and push down delamination were analyzed, which was further used to study the candle stick drills.

## 2 Drilling experiments


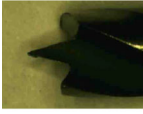
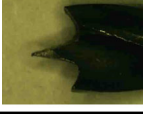
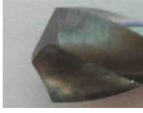
### 2.1 Machine setup

The GFRP laminate was mounted on a dynamometer. There was a plastic backup plate between the laminate and the dynamometer. The backup plate was used to protect the dynamometer, when the laminate was drilled through. There were many pilot holes in the backup plate to avoid drilling into the backup plate. The dynamometer was mounted on a table of the numerically controlled (NC) milling machine. Drilling forces were measured using the piezoelectric dynamometer (Kistler 9257A). The signals were collected by a data acquisition system which included a dual mode amplifier (Kistler 5004) and Kistler Dynoware software. Measurements were obtained with a frequency of 200 Hz throughout the drilling process. Finally, the complete experimental platform is shown in Fig. 1. At the same time, microscopy was the most easily accessible and economical technique for measuring delamination damage, the UNION optical microscope used in the paper is shown in Fig. 2.

### 2.2 Material specification

Quasi-anisotropic GFRP laminate used in the article had a dimension of 74 mm × 65 mm × 5.25 mm. The main performance parameters are described in Table 1 and Table 2.

**Table 3** Geometric angles for candle stick drills and twist drill <sup>(a)</sup>Measured at the outer diameter

No. of drill	Drill	Rake angle of inner cutting edge ( $\gamma_i$ )	Clearance angle of inner cutting edge ( $\alpha_i$ )	Inner drill tip angle ( $2\Phi$ )	Rake angle of outer cutting edge ( $\gamma_o$ ) <sup>a</sup>	Clearance angle of outer cutting edge ( $\alpha_o$ )	Outer drill tip angle ( $2\Phi'$ )
1 <sup>#</sup>		10°	45°	70°	30°	50°	180°
2 <sup>#</sup>		5°	10°	45°	25°	20°	210°
3 <sup>#</sup>		0°	0°	25°	20°	3°	210°
No. of drill	Drill	Rake angle <sup>a</sup>		Clearance angle <sup>a</sup>		Tip angle	
4 <sup>#</sup>		30°		40°		120°	

### 2.3 Drill tools

According to the candle stick drills used in the references [14, 19, 21, 33, 34], the specific geometry of the candle stick drill marked with professional terms is shown in Fig. 3. The candle stick drill consisted of the three drill tips and the four cutting edges. There were one inner drill tip, two outer drill tips, two inner cutting edges, and two outer cutting edges. The cutting edges had the corresponding rake angle and clearance angle. The angle between the two inner cutting edges was the inner drill tip angle ( $2\Phi$ ). The angle between the two outer cutting edges was the outer drill tip angle ( $2\Phi'$ ). The distance between the inner and the outer drill tips in axial direction was the distance ( $h$ ). In this paper, three common commercial candle stick drills [17–20] and a traditional twist drill were used as experimental tools. The geometry of three candle stick drills used in this study is shown in Fig. 4. The maximum horizontal distance between the two inner cutting edges for all three candle stick drills was 2 mm. Finally, the measured values of rake angles, clearance angles, and drill tip angles for three candle stick drills and twist drill with a diameter of 6 mm are described in Table 3.

### 2.4 Machining plan and parameters

In this paper, two drilling tests were proceeded by each candle stick drill. The first test was normal drilling without pilot hole. The second test was drilling under a pilot hole with a diameter

of 2 mm. One drilling test was proceed by the twist drill. Finally, the specific experimental plan and machining parameters are shown in Table 4.

### 2.5 Delamination factor

Chen [35] first proposed the concept of the delamination factor (i.e., the ratio of the maximum diameter  $D_{max}$  in the damage zone to the hole diameter ( $D$ ), namely the conventional delamination factor ( $F_a$ ), to easily analyze and compare the degree of delamination in drilling CFRP composite laminates. The equation of the conventional delamination factor around the holes measured by using a UNION optical microscope can be expressed as the following:

$$F_a = \frac{D_{max}}{D} \quad (1)$$

**Table 4** Experimental plan and machining parameters

Expt. no.	Drill no.	Pilot hole and its diameter (mm)	Feed speed (mm/min)	Spindle speed r/min)
1	1 <sup>#</sup>	–	200	2000
2	2 <sup>#</sup>	–		
3	3 <sup>#</sup>	–		
4	1 <sup>#</sup>	2		
5	2 <sup>#</sup>	2		
6	3 <sup>#</sup>	2		
7	4 <sup>#</sup>	–		

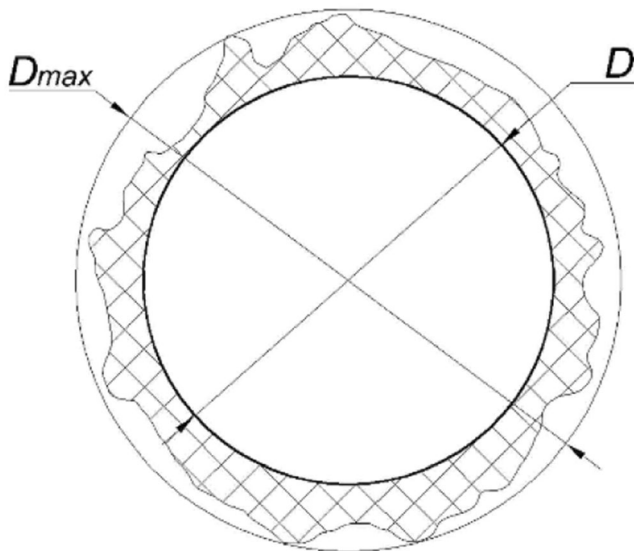


Fig. 5 Scheme of delamination

where  $D$  represents the actual diameter for drilled hole or drill and  $D_{max}$  represents the maximum diameter for delamination area, as shown in Fig. 5.

### 3 Finite element model of drilling

In this paper, 3D finite element (FE) models, which are based on Lagrangian formulation, were developed to simulate the drilling process. Commercial finite element software Abaqus/explicit was used. The mass and inertia effects were included in the models. Due to the dynamic characteristics of the process, dynamic explicit finite element integration has been used in the paper. The models were aimed at simulating the drilling process, which further to predict the character and extent of push down delamination at the exit surface of the laminate. A user-defined 3D damage model (VUMAT) with solid elements was developed and implemented into the finite code Abaqus/explicit [36]. The general contact algorithm in Abaqus/explicit was used to simulate contact conditions between the candle stick drills and the composite laminates. An element deletion approach [37] was used to represent the hole-making process based on initiation and evolution of damage in the meshed GFRP elements.

Table 5 Orthotropic unidirectional material properties

Property	Value	Property	Value
$E_{11}$ (GPa)	20.6	$E_{22} = E_{33}$ (GPa)	17.2
$G_{12} = G_{13}$ (GPa)	4.5	$G_{23}$ (GPa)	3
$\nu_{12} = \nu_{13}$	0.3	$\nu_{23}$	0.4
$\rho$ (kg/m <sup>3</sup> )	2540		

Table 6 Damage parameters

Property	Value	Property	Value
$\sigma_{11}^{f,T}$ (MPa)	1034	$\sigma_{11}^{f,C}$ (MPa)	1034
$\sigma_{22}^{f,T}$ (MPa)	27.6	$\sigma_{22}^{f,C}$ (MPa)	138
$\sigma_{33}^{f,T}$ (MPa)	27.6	$\sigma_{33}^{f,C}$ (MPa)	138
$\tau_{12}^f$ (MPa)	41.4	$\tau_{13}^f$ (MPa)	69
$\tau_{23}^f$ (MPa)	69		

### 3.1 Stress model

Orthotropic material properties were assigned to each unidirectional composite lamina according to the fiber orientation by using a pre-defined local coordinate system. Linear elastic material behavior was assumed prior to any damage for each element and it can be calculated as following.

$$[\sigma] = [C][\varepsilon] \tag{2}$$

The material properties of UD-GFRP are given in Table 5.

### 3.2 Damage initiation

The damage initiation criteria for FRP composites were based on Hashin’s theory [38]. The initiation behavior was also assumed to be orthotropic and the initiation criteria considered four different damage initiation mechanisms, namely fiber tension, fiber compression, matrix tension, and matrix compressing. These four initiation criteria are described as followings.

fiber tension ( $\sigma_{11} > 0$ )

$$F_f^T = \left(\frac{\sigma_{11}}{\sigma_{11}^{f,T}}\right)^2 + \alpha \left(\frac{\tau_{12}}{\tau_{12}^f}\right)^2 + \beta \left(\frac{\tau_{13}}{\tau_{13}^f}\right)^2 \tag{3}$$

fiber compression ( $\sigma_{11} \leq 0$ )

$$F_f^C = \left(\frac{\sigma_{11}}{\sigma_{11}^{f,C}}\right)^2 \tag{4}$$

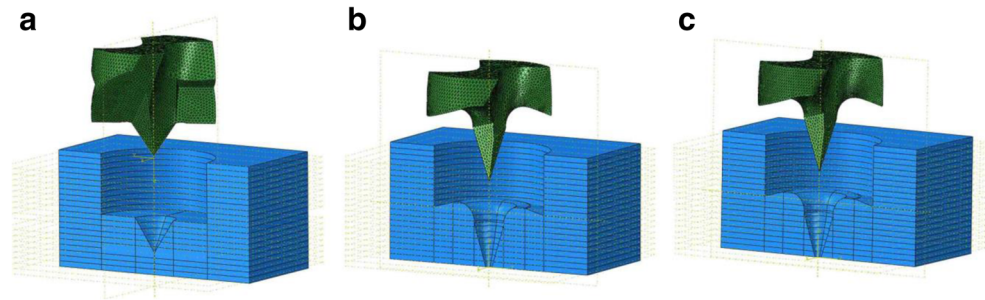
matrix tension ( $\sigma_{22} + \sigma_{33} > 0$ )

$$F_m^T = \left(\frac{1}{\sigma_{22}^{f,T}}\right)^2 (\sigma_{22} + \sigma_{33})^2 + \left(\frac{1}{\sigma_{23}^{f,T}}\right)^2 (\tau_{23}^2 - \sigma_{22}\sigma_{33}) + \left(\frac{1}{\tau_{12}^f}\right)^2 (\tau_{12}^2 + \tau_{13}^2) \tag{5}$$

matrix compression ( $\sigma_{22} + \sigma_{33} \leq 0$ )

$$F_m^C = \left(\frac{1}{\sigma_{22}^{f,C}}\right)^2 \left[ \left(\frac{\sigma_{22}^2}{2\tau_{23}^2}\right)^2 - 1 \right] (|\sigma_{22} + \sigma_{33}|) + \left(\frac{1}{2\tau_{23}^f}\right)^2 (\sigma_{22} + \sigma_{33})^2 + \left(\frac{1}{\tau_{23}^f}\right)^2 (\tau_{23}^2 - \sigma_{22}\sigma_{33}) + \left(\frac{1}{\tau_{12}^f}\right)^2 (\tau_{12}^2 + \tau_{13}^2) \tag{6}$$

**Fig. 6** FE models of drilling GFRP with candle stick drills. **a** 1<sup>#</sup>. **b** 2<sup>#</sup>. **c** 3<sup>#</sup>



Where *m* and *f* subscripts denote matrix and fiber; *C* and *T* represent compression and tension, and *f* superscript denotes failure, respectively.  $\sigma$  and  $\tau$  are the normal and shear stresses, respectively. The damage parameters are given in Table 6.

**3.3 Damage evolution**

When the Hashin criteria have been fulfilled in any mode, damage has been initiated. In this paper, a sudden degradation criterion was applied for the evolution of the laminate damage in any mode.

$$[\bar{\sigma}] = [\bar{C}][\varepsilon] \tag{7}$$

The damage variables of damaged stiffness matrix ( $\bar{C}$ ) for a particular mode can be defined as reported in the following equations:

$$d_f = \begin{cases} 0 & \text{if } \bar{\sigma}_{11} > 0 \text{ and } F_f^T < 1 \\ 1 & \text{if } \bar{\sigma}_{11} > 0 \text{ and } F_f^T \geq 1 \\ 0 & \text{if } \bar{\sigma}_{11} \leq 0 \text{ and } F_f^C < 1 \\ 1 & \text{if } \bar{\sigma}_{11} \leq 0 \text{ and } F_f^C \geq 1 \end{cases} \tag{8}$$

$$d_m = \begin{cases} 0 & \text{if } \bar{\sigma}_{22} + \bar{\sigma}_{33} > 0 \text{ and } F_m^T < 1 \\ 1 & \text{if } \bar{\sigma}_{22} + \bar{\sigma}_{33} > 0 \text{ and } F_m^T \geq 1 \\ 0 & \text{if } \bar{\sigma}_{22} + \bar{\sigma}_{33} \leq 0 \text{ and } F_m^C < 1 \\ 1 & \text{if } \bar{\sigma}_{22} + \bar{\sigma}_{33} \leq 0 \text{ and } F_m^C \geq 1 \end{cases} \tag{9}$$

$$d_s = 1 - (1 - d_f)(1 - d_m) \tag{10}$$

**3.4 Geometry, mesh, and elements**

3D FE models of drilling were developed, which consisted of three candle stick drills and GFRP composite laminates with appropriate boundary conditions, as shown in Fig. 6.

**Table 7** The material properties of tungsten carbide drills

Property	Value	Property	Value
<i>E</i> (GPa)	580	$\nu$	0.22
$\rho$ (kg/m <sup>3</sup> )	14,500		

GFRP laminates having a dimension of 12 mm × 6 mm × 5.25 mm consisted of 21 plies having a stacking sequence of 0° [−45° 90° 45° 0°]<sub>3S</sub> 0°. Three candle stick drills with a diameter of 6 mm were modeled and imported into the FE simulation. According to the shapes of three candle stick drill tips, three blind holes which kept 10 layers undrilled at the bottom of the laminate were precast in the laminates. Initially, cutting tools were assumed fully elastic materials to calculate the mass and inertia in the FE models. Then the drills were modeled as rigid bodies. Mass and inertia were still added to these rigid drills to simulate equivalent kinematics of the process. The use of rigid tools in the FE simulation would decrease computational time and maintain the efficiency of the FE analysis. The mesh size of the laminates was refined in the drilling area and the high-stress gradient locus to model the process accurately. The laminates were modeled using reduced-integrated 8-noded brick elements (C3D8R) and the tetrahedral elements (C3D4) were used in three candle stick drills.

**3.5 Boundary conditions and loading**

The laminates were fixed from the bottom surfaces. At the beginning of the FE simulation, the drills were located at the center of the area to be drilled. The drills were restrained along its axis (*UX* = *UY* = *URX* = *URY* = 0) so that the drills can only move along the feed direction. The drill bits had a spindle speed (*VRZ* = 2000 r/min) and a feed speed (*VZ* = 200 mm/min) as process parameters.

**3.6 Material properties**

The material parameters of laminates are described in Table 5. The material parameters of three candle stick drills are given in Table 7.

**3.7 Drills-laminates contact**

The contact and friction parameters used in the simulations were based on a number of experimental factors such as

**Table 8** Experimental parameters and results

Expt. no.	Drill no.	Pilot hole and its diameter (mm)	Feed speed (rpm)	Spindle feed (mm/min)	Thrust force (N)	Peel up delamination	Push down delamination
1	1 <sup>#</sup>	–	200	2000	84	1.0887	1.4441
2	2 <sup>#</sup>	–			477.3	1.1316	1.3150
3	3 <sup>#</sup>	–			894	1.1499	1.3901
4	1 <sup>#</sup>	2			50.46	–	–
5	2 <sup>#</sup>	2			328.3	–	–
6	3 <sup>#</sup>	2			475.84	–	–
7	4 <sup>#</sup>	–			67.3	1.1254	1.3233

spindle speed, feed speed, drill tip geometries, and material properties. Contacts between three candle stick drills and the GFRP laminates were defined by the general contact algorithm available in Abaqus/explicit. This algorithm generated the contact forces based on the penalty-enforced contact method. The friction coefficient  $\mu$  was used to account for the shear stress of the surface traction  $\tau$  with the contact pressure  $p$  and can be represented as  $\tau = \mu p$ . In this case, the frictional contact between drills and composite laminates was modeled with a constant coefficient of friction of 0.3 [39].

### 4 Results and discussion

The experimental numbers, experimental tools, machining parameters, thrust forces, and delamination factors for peel up delamination and push down delamination are listed in Table 8. As shown in Table 8, compared with the twist drill of 4<sup>#</sup>, all three candle stick drills obtained relatively larger

thrust force. What is more, the candle stick drill of 1<sup>#</sup> got less peel up delamination, but worse push down delamination than twist drill. The candle stick drill of 2<sup>#</sup> obtained smaller push down delamination, but larger peel up delamination than twist drill. The candle stick drill of 3<sup>#</sup> gained more severe peel up and push down delamination than twist delamination.

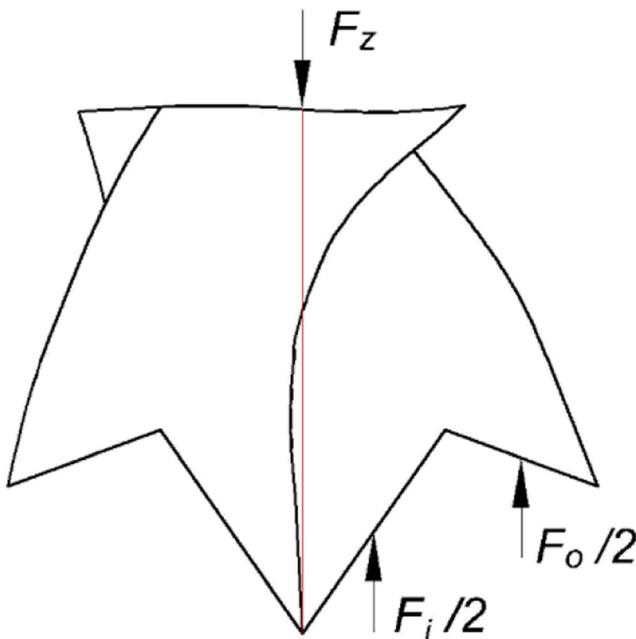
Compared to the twist drill, the candle stick drill had a smaller center than the chisel edge of twist drill. At the same time, in addition to the concentrated center load at the center of drill, the candle stick drill mainly also had the distributed circular load toward the drill periphery under the action of the outer cutting edges. That is to say, the geometry of the outer cutting edge allowed the cutting action to happen from the outer to the inner tool diameter, similarly to a trepanning tool. Due to the existence of the above structural features, related researches [10, 14, 23] showed that candle stick drills could achieve lower thrust force, peel up, and push down delamination than twist drill. But the experimental results in this paper showed that not all candle stick drills could get good drilling quality and further revealed that the geometric angles of the drill tip might have a significant impact on the quality of the drilling.

#### 4.1 Thrust forces for candle stick drills

The thrust force during drilling came from the inner cutting edges and the outer cutting edges due to the special geometry of the candle stick drill. As shown in Fig. 7, the total thrust force is  $F_z$ , the thrust force generated by the inner cutting edges is  $F_i$ , and the thrust force generated by the outer cutting edges is  $F_o$ . The relationship between them is described below.

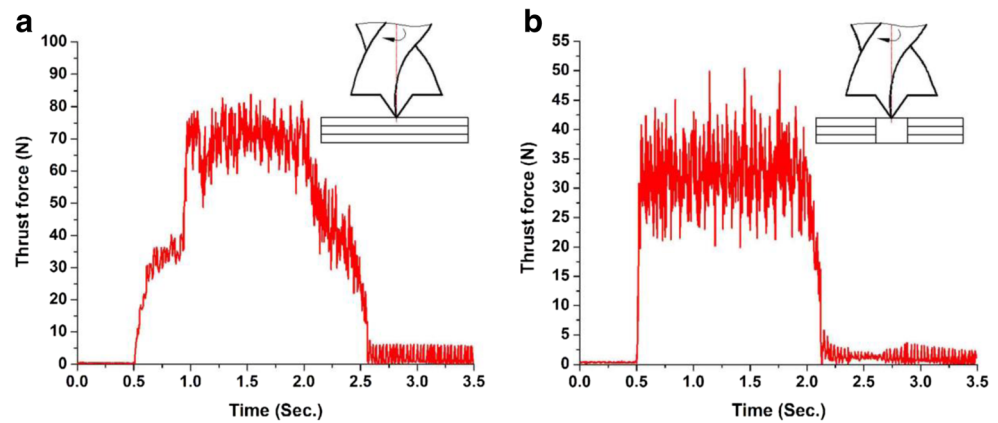
$$F_z = F_i + F_o \tag{11}$$

According to the machining plan and parameters, two drilling tests were proceeded by each drill. The first test was normal drilling without pilot hole, and the second test was drilling under a pilot hole with a diameter of 2 mm. The typical thrust force curves recorded during drilling are shown in Fig. 8. Figure 8a shows the thrust force during drilling



**Fig. 7** Thrust force distribution of candle stick drill

**Fig. 8** Typical thrust forces signal recorded during drilling using candle stick drill. **a** Without pilot hole. **b** Under a pilot hole with a diameter of 2 mm



without pilot hole, that is, the thrust force  $F_z$  during drilling under the full effect of the inner and outer cutting edges. Figure 8b shows the thrust force during drilling under a pilot hole with a diameter of 2 mm, that is, the thrust force  $F_o$  during drilling under the only effect of the outer cutting edges.

For the two drilling tests were proceeded by each drill, the maximum thrust force generated by the normal drilling without pilot hole was  $F_{z-max}$ . The maximum thrust force generated by the drilling under a pilot hole with a diameter of 2 mm was  $F_{o-max}$ . The maximum thrust force ( $F_{i-max}$ ) generated by the only inner cutting edges was equal to the  $F_{z-max}$  minus the  $F_{o-max}$ . Finally, the thrust force ( $F_{z-max}$ ), the thrust force ( $F_{o-max}$ ) and its proportion in the thrust force ( $F_{z-max}$ ), and the thrust force ( $F_{i-max}$ ) and its proportion in the thrust force ( $F_{z-max}$ ) for the three candle stick drills are listed in Table 9. Figure 9 shows the changing trends of the thrust forces ( $F_{z-max}$ ), ( $F_{o-max}$ ), and ( $F_{i-max}$ ) with the change in drills.

For the thrust force ( $F_{i-max}$ ), the  $F_{i-max}$  was increased with the change in the inner cutting edge of candle stick drill. From the 1<sup>#</sup> to the 3<sup>#</sup>, the inner drill tip angle ( $2\Phi$ ) was decreased from  $70^\circ$  to  $25^\circ$ , the rake angle of inner cutting edge ( $\gamma_i$ ) was decreased from  $10^\circ$  to  $0^\circ$ , and the clearance angle of inner cutting edge ( $\alpha_i$ ) was decreased from  $45^\circ$  to  $0^\circ$ . Within 180 degrees, the inner drill tip angle was same as the point angle involved in many literatures, and the thrust force was decreased with the reduction in the point angle [28, 29, 31]. At the same time, the thrust force was increased with the reduction in the rake and clearance angles of the inner cutting edge. From the 1<sup>#</sup> to the 3<sup>#</sup>, the  $F_{i-max}$  was increased, and the maximum increase was 1316% according to Table 9. The minimum thrust force ( $F_{i-max}$ ) achieved by the drill of 1<sup>#</sup> was

mainly due to its relatively larger rake and clearance angles of inner cutting edge, but not the inner drill tip angle. The drill of 3<sup>#</sup> obtained the maximum thrust force ( $F_{i-max}$ ), which was attributed to its rake and clearance angles of  $0^\circ$  for the inner cutting edge, not for its inner drill tip angle. These findings indicated that the change in the thrust force ( $F_{i-max}$ ) generated by the inner cutting edges was more sensitive to the rake and clearance angles of the inner cutting edge.

For the thrust force ( $F_{o-max}$ ), the  $F_{o-max}$  was increased with the change in the outer cutting edge of candle stick drill. From the 1<sup>#</sup> to the 3<sup>#</sup>, the outer drill tip angle ( $2\Phi'$ ) was increased from  $180^\circ$  to  $210^\circ$ , the rake angle of outer cutting edge ( $\gamma_o$ ) was decreased from  $30^\circ$  to  $20^\circ$ , and the clearance angle of outer cutting edge ( $\alpha_o$ ) was decreased from  $50^\circ$  to  $3^\circ$ . When the angle was greater than 180 degrees, the outer drill tip angle was same as the point angle involved in some literature. The thrust force was increased with the increase in the point angle, and the largest increase was 25% within the changing range of 10 degrees from  $175^\circ$  to  $185^\circ$  [32]. The thrust force was also increased with the reduction in the rake and clearance angles of the outer cutting edge. For the three candle stick drills, the rake face of the outer cutting edge was formed by the spiral flute, that is, the rake angle of outer cutting edge was same as the helix angle. At the same time, the thrust force was increased with the reduction in the helix angle, and the maximum increase was 7% within the changing range of 16 degrees from  $40^\circ$  to  $24^\circ$  [28]. So, within the changing range of 10 degrees from  $30^\circ$  to  $20^\circ$ , the change in the rake angle of outer cutting edge had limited and relatively small influence on the thrust force ( $F_{o-max}$ ) for the three candle stick drills in this paper. From the 2<sup>#</sup> to the 3<sup>#</sup>, the clearance angle of outer

**Table 9** Experimental thrust force distribution for three candle stick drills

Drill	Feed speed (mm/min)	Spindle speed (r/min)	$F_{z-max}$ (N)	$F_{o-max}$ (N) (portion)	$F_{i-max}$ (N) (portion)
1 <sup>#</sup>	200	2000	84	50.46 (60.1%)	29.54 (39.9%)
2 <sup>#</sup>			477.3	328.3 (68.8%)	149 (31.2%)
3 <sup>#</sup>			894	475.84 (53.2%)	418.16 (46.8%)



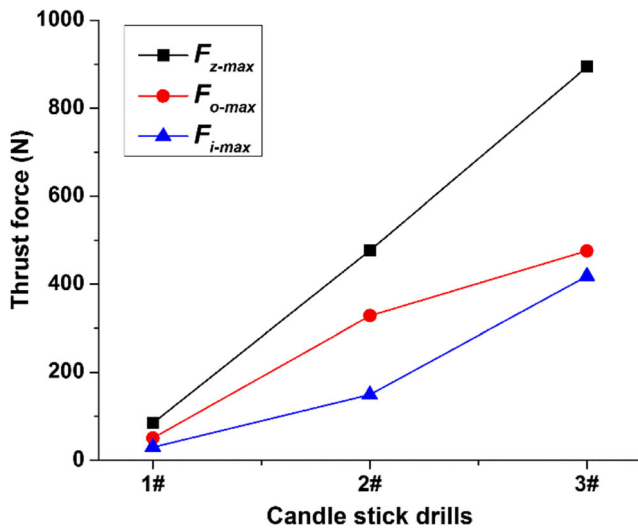
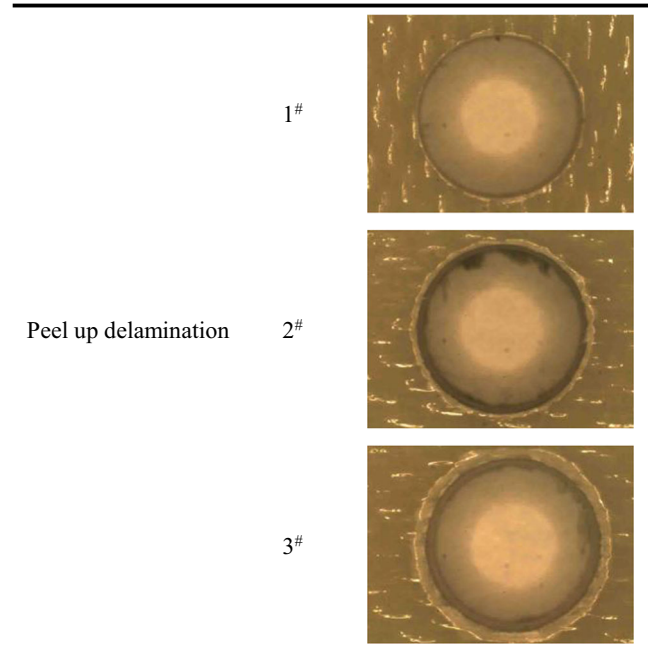


Fig. 9 Thrust forces with three candle stick drills

cutting edge was decreased from 20° to 3°. The outer drill tip angle was 210° for all the drills of the 2# to the 3#. From the 2# to the 3#, the  $F_{o-max}$  was increased, and the increase was 45% from 475.84 to 328.3 N according to Table 9. These analyses indicated that the clearance angle of the outer cutting edge had an important impact on the thrust force ( $F_{o-max}$ ). The minimum thrust force ( $F_{o-max}$ ) for the drill of 1# was mainly resulting from the relatively larger clearance angle of outer cutting edge and relatively smaller outer drill tip angle.

For the thrust force ( $F_{z-max}$ ), the  $F_{z-max}$  was increased with the candle stick drill changing. According to the above analysis, this was mainly due to the reduction in the rake and clearance angles of the inner cutting edge, the reduction in the clearance angle of the outer cutting edge, and the increase in the outer drill tip angle with the candle stick drill changing. As given in Table 8, the proportion of the thrust force ( $F_{o-max}$ ) in the thrust force ( $F_{z-max}$ ) was greater than 50% for all the three candle stick drills. This indicated that the thrust force ( $F_{z-max}$ ) was mainly derived from the outer cutting edges. Then, it is further learned from the analytical results of the

Table 10 Peel up delamination at the entrance surface of the hole for three candle stick drills.



thrust force ( $F_{o-max}$ ) that the clearance angle of the outer cutting edge and the outer drill tip angle had a significant impact on the thrust force ( $F_{z-max}$ ). For the drill of 3#, the thrust force ( $F_{o-max}$ ) and ( $F_{i-max}$ ) were similar, and their proportions in the thrust force ( $F_{z-max}$ ) were also similar. This may be mainly due to the rake and clearance angles of 0° for the inner cutting edges.

### 4.2 Delamination for candle stick drills

#### 4.2.1 Peel up delamination

For the candle stick drills used in this article, the inner drill tip first got engaged with the laminate at the

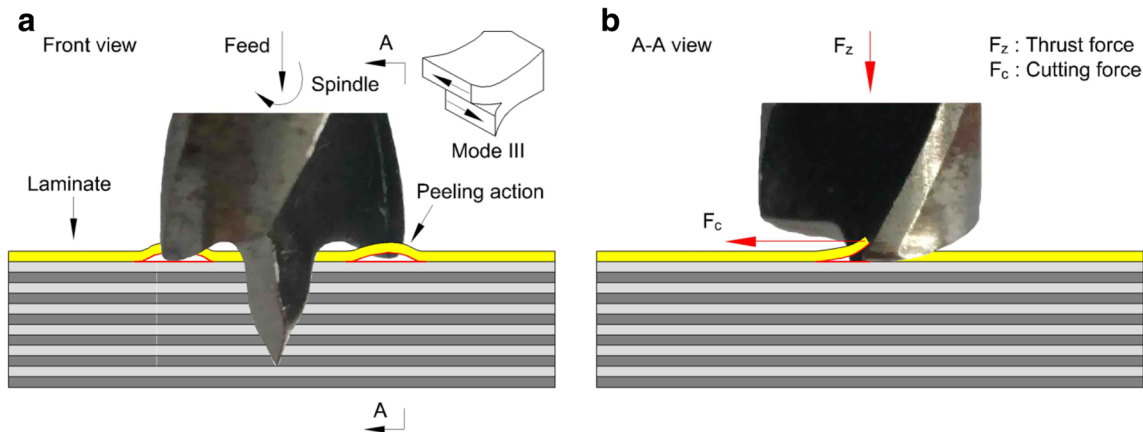


Fig. 10 Mechanism of peel up delamination. a Front view. b A-A view

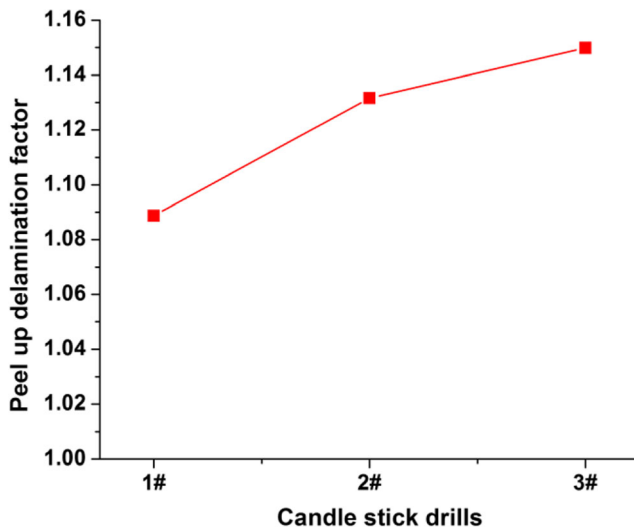


Fig. 11 Peel up delamination factors with three candle stick drills

beginning of the drilling. Moreover, the inner drill tip served on a pilot drill and entered the laminate lightly. The drilling track of the inner drill tip was accurate, which would not be deflected from the influence of different densities of the fibers and resin in composite. For the drill of 1#, the drilling behavior occurred simultaneously throughout the length of the outer cutting edge when the outer cutting edge begin to cut the laminate, which further formed the entrance surface of the hole. For the drills of 2# and 3#, when the outer cutting edge begin to cut the laminate, the drilling behavior typically and first taken place in the position where the outer drill tip and the laminate was in contact, which further formed the entrance surface of the hole. So, the entrance surface quality of the hole was mainly depended on the outer cutting edge for the three candle stick drills. That is, the peel up delamination at the entrance surface of the hole was also mainly derived from the outer cutting edge. Previous studies have demonstrated the mechanism of the peel up delamination [1, 4]. Figure 10 shows the mechanism of the peel up delamination at the entrance surface of the hole under the drilling action of the outer

cutting edges, (a) front view and (b) A-A view. The front view shows the fiber peeling action at the entrance surface of the laminate under the drilling behavior of the outer cutting edges. A-A view shows the cutting force upwards to separate the upper laminas from the uncut portion held by the downward acting thrust force. So, as shown in Fig. 10, the outer cutting edges of the candle stick drill will abrade the laminate. It then, by moving forward, tends to pull the abraded material away along the flute. The material spirals up before it is machined completely. This action introduces a peeling force upwards to separate the upper laminas from the uncut portion held by the downward acting thrust force ( $F_z$ ). The cutting force ( $F_c$ ) acting in the peripheral direction is the driving force for delamination by fracture in Mode III loading. It generates a peeling force in the axial direction through the slope of the drill flute and is a function of tool geometry and friction between the tool and laminate. Delamination caused by peel-up becomes progressively more difficult as drilling proceeds, since the thickness resisting the lamina bending becomes greater.

For the three candle stick drills used in this paper, when the outer cutting edges began to cut the laminate, the cutting force ( $F_c$ ) was mainly derived from the rake angle of outer cutting edge and the outer drill tip angle. The thrust force ( $F_z$ ) was mainly derived from the outer drill tip angle and the clearance angle of outer cutting edge. The cutting force ( $F_c$ ) acting in the peripheral direction is the driving force for the peel up delamination. So, the influence of the outer cutting edge on the peel up delamination was mainly concentrated in the rake angle of outer cutting edge and the outer drill tip angle.

Peel up delamination at the entrance surface of the hole after drilling is shown in Table 10. Peel up delamination factors for the three candle stick drills are shown in Fig. 11. The peel up delamination was increased with the change in the candle stick drill. With the change in the drill, the outer drill tip angle ( $2\phi'$ ) was increased from  $180^\circ$  to  $210^\circ$ , and the rake angle of outer cutting edge ( $\gamma_o$ ) was decreased from  $30^\circ$  to  $20^\circ$ . Peel up delamination had a great relationship with the

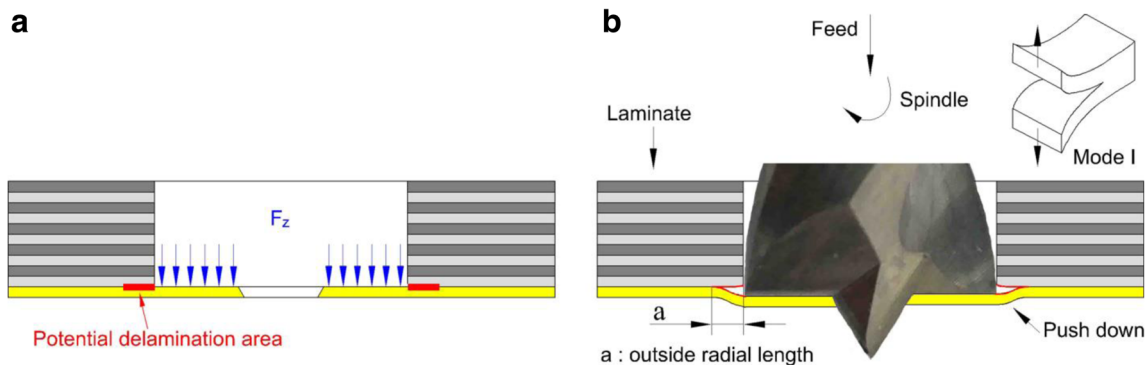


Fig. 12 Mechanism of push down delamination for the drill of 1#

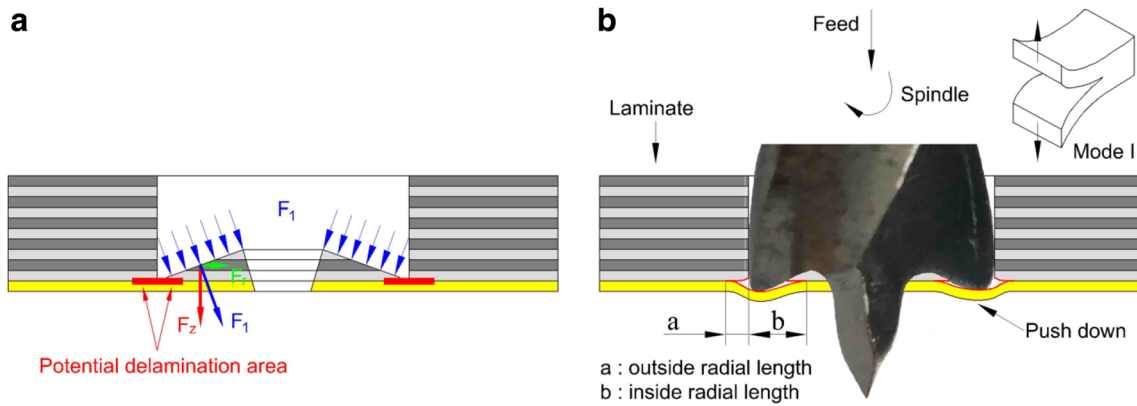


Fig. 13 Mechanism of push down delamination for the drills of 2# and 3#

rake angle of cutting edge and point angle [31, 32]. That is, the drill whose point angle was greater than 180 degrees could obtain relatively good peel up delamination. The drill with this point angle firstly cut the material using the outer area of the drill and therefore led to the relatively good results regarding peel up delamination at the entrance. And the peel up delamination was increased with the reduction in the rake angle of cutting edge. For the three candle stick drills, the peel up delamination was gradually increased with the changing in the outer cutting edge of candle stick drill. Above analysis indicated the contribution of the rake angle of outer cutting edge to the peel up delamination was greater than the outer drill tip angle. That is to say, the minimum peel up delamination achieved by the drill of 1# was mainly due to its relatively larger rake angle of outer cutting edge. The drill of 3# obtained

the maximum peel up delamination, which was attributed to its relatively smaller rake angle of outer cutting edge.

### 4.3 Push down delamination

Previous studies have demonstrated the mechanism of push down delamination [1, 4]. The drill always exerts a compressive thrust force on the laminate in drilling. The laminate under the drill thus tends to be drawn away from the interlaminar bond around the hole. As the drilling approaches the end, the uncut thickness becomes smaller and the resistance to deformation decreases. At some point, the loading exceeds the interlaminar bond strength and delamination occurs by fracture in Mode I loading. This happens before the laminate is completely penetrated by the drill. For the drills used in this article, it is greatly clear from the analysis of thrust force that the thrust force generated by the candle stick drills was mainly derived from the outer cutting edges. At the same time, most of the inner cutting edges had drilled through the laminate as the drilling came to an end. So, the compressive thrust force, causing the push down delamination at the exit surface of the

Table 11 Push down delamination at the exit surface of the hole for three candle stick drills.

	1#	
Push down delamination	2#	
	3#	

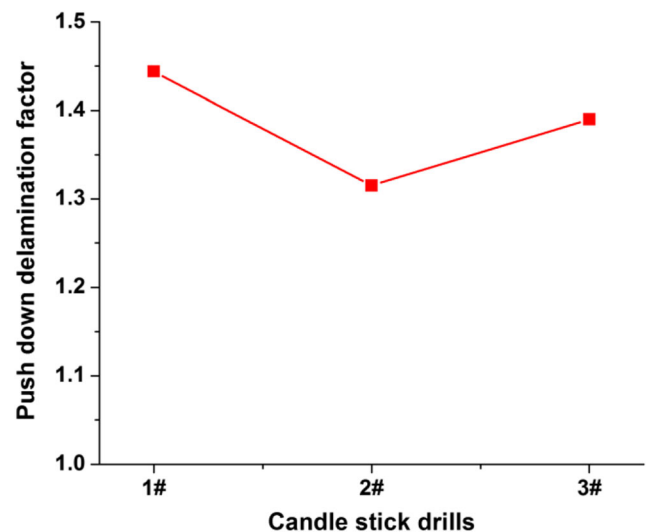
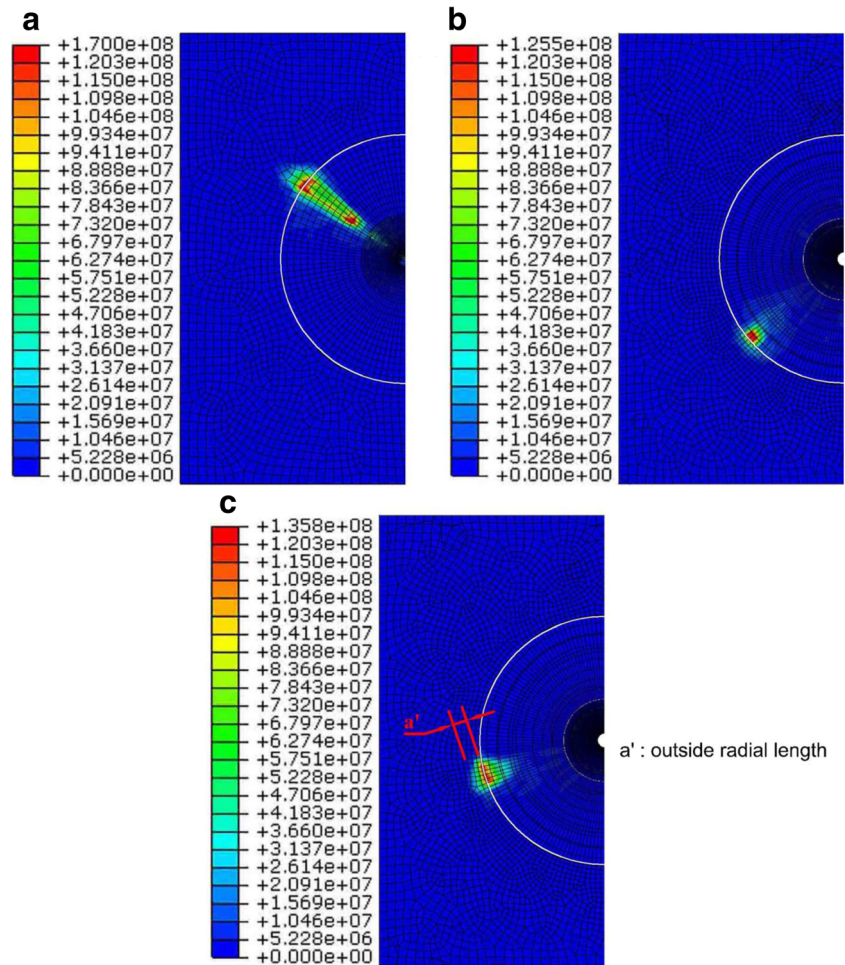


Fig. 14 Push down delamination factors with three candle stick drills

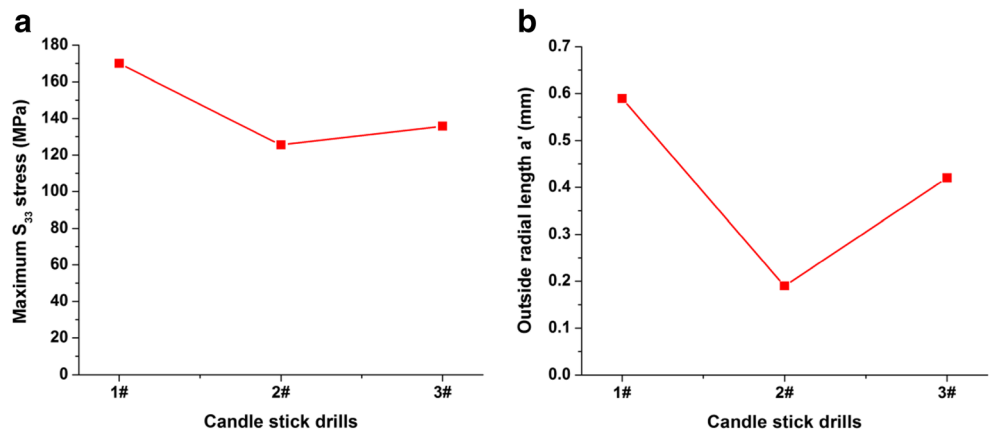
**Fig. 15** Axial  $S_{33}$  stress distribution with the three candle stick drills. **a** 1<sup>#</sup>. **b** 2<sup>#</sup>. **c** 3<sup>#</sup>



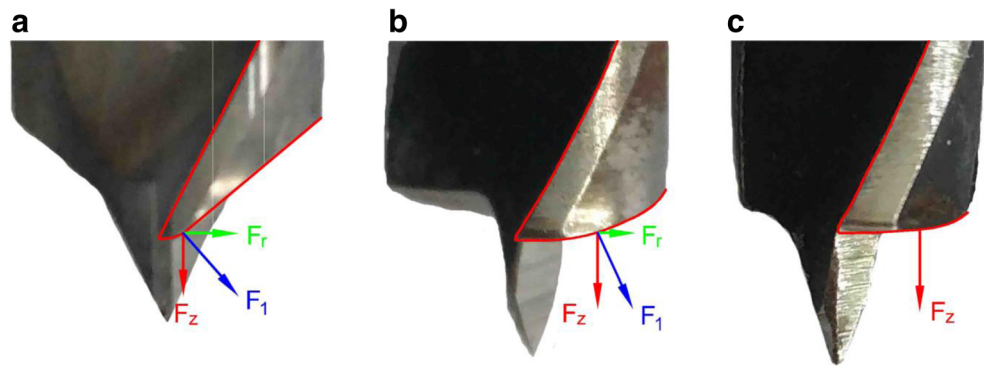
hole, was resulting from the outer cutting edges. That is, the push down delamination mainly came from the outer cutting edges. Also, the thrust force generated by the outer cutting edge was mainly resulting from the outer drill tip angle and the clearance angle of outer cutting edge. So, the influence of the candle stick drill on the push down delamination was mainly concentrated in the outer drill tip angle and the clearance angle of outer cutting edge.

Figure 12 shows the mechanism of the push down delamination at the exit surface of the hole under the compressive thrust force generated by the outer cutting edges for the drill of 1<sup>#</sup>. So, as shown in Fig. 12, the area of loading concentration under the action of thrust force was at the outside of the hole. That is, the potential delamination area was concentrated on the outside of the hole. Push down delamination occurred when the loading exceeds the interlaminar bond strength and

**Fig. 16 a** Maximum axial  $S_{33}$  stress values and **b** outside radial lengths  $a'$  of the stress distribution at the outside of the hole with the three candle stick drills



**Fig. 17** Thrust force under the action from the clearance angle of outer cutting edge with candle stick drills. **a** 1<sup>#</sup>. **b** 2<sup>#</sup>. **c** 3<sup>#</sup>



extended along the outside of the hole, which further formed the outside radial length ( $a$ ) in the area of push down delamination.

Figure 13 shows the mechanism of the push down delamination at the exit surface of the hole under the compressive thrust force generated by the outer cutting edges for the drills of 2<sup>#</sup> and 3<sup>#</sup>. So, as shown in Fig. 13, the area of loading concentration under the action of thrust force was at the both sides of the outer drill tip. That is, the potential delamination area was mainly concentrated on the both sides of the outer drill tip. Push down delamination occurred when the loading exceeds the interlaminar bond strength and extended along the both sides of the outer drill tip, which further formed the outside radial length ( $a$ ) and inside radial length ( $b$ ) in the area of push down delamination.

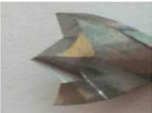
Push down delamination at the exit surface after drilling are shown in Table 11. Push down delamination factors with three candle stick drills are shown in Fig. 14. The push down delamination for the 1<sup>#</sup> is greater than that for the 2<sup>#</sup> and 3<sup>#</sup>, and push down delamination for the 3<sup>#</sup> is greater than that for the 2<sup>#</sup>. Figure 15 shows the results of simulated axial  $S_{33}$  stress distribution with the three candle stick drills, (a) 1<sup>#</sup>, (b) 2<sup>#</sup>, and (c) 3<sup>#</sup>. In the case of the same contact thickness between the three candle stick drills and the laminate, the axial  $S_{33}$  stress distribution was extracted from the plane where the contact points between the outer drill tips and the laminate were located. So, as shown in Fig. 15, the white semicircle line was the dividing line between the inside and outside of the drilling

hole. The area surrounded by the white semicircle line was the inside of the drilling hole, and another area was the outside of the drilling hole. The size of the axial  $S_{33}$  stress value represented the susceptibility of the adhesive layer to damage. The greater stress value, the easier the adhesive layer was to be destroyed, that is, the easier delamination would occur. The outside radial length ( $a'$ ) of the stress distribution at the outside of the hole represented the potential outside radial length of the delamination extension. That is, the longer outside radial length of the stress distribution, the longer outside radial length of the delamination damage.

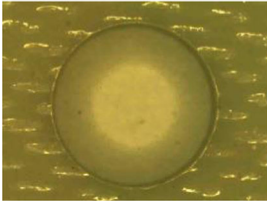
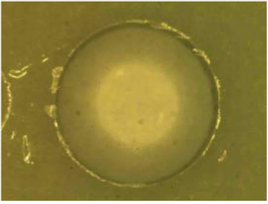
The maximum axial  $S_{33}$  stress values and the outside radial lengths ( $a'$ ) of the stress distribution at the outside of the hole for the three candle stick drills are shown in Fig. 16. So, as shown in Fig. 16, the maximum axial  $S_{33}$  stress value and the outside radial length of the stress distribution for the 1<sup>#</sup> are significantly larger than that for the 2<sup>#</sup> and 3<sup>#</sup>. That is, the push down delamination for the 1<sup>#</sup> is greater than that for the 2<sup>#</sup> and 3<sup>#</sup>. At the same time, the maximum axial  $S_{33}$  stress value and the outside radial length ( $a'$ ) for the 3<sup>#</sup> are larger than that for the 2<sup>#</sup>. That is to say, the push down delamination for the 3<sup>#</sup> is greater than that for the 2<sup>#</sup>. So, the maximum axial  $S_{33}$  stress value and the outside radial length of the stress distribution at the outside of the hole could well reflect and explain the push down delamination for these three candle stick drills in theory.

With the change in the candle stick drill, the outer drill tip angle ( $2\Phi'$ ) was increased from  $180^\circ$  to  $210^\circ$ , and the

**Table 12** Optimized the geometric angles of candle stick drill (<sup>a</sup>Measured at the outer diameter)

Drill	Rake angle of inner cutting edge ( $\gamma_i$ )	Clearance angle of inner cutting edge ( $\alpha_i$ )	Inner drill tip angle ( $2\Phi$ )	Rake angle of outer cutting edge ( $\gamma_o$ ) <sup>a</sup>	Clearance angle of outer cutting edge ( $\alpha_o$ )	Outer drill tip angle ( $2\Phi'$ )
	10°	45°	70°	30°	50°	220°

**Table 13** Verification test results

Feed speed (rpm)	Spindle feed (mm/min)	Thrust force (N)	Peel up Delamination	Peel up delamination factor	Push down delamination	Push down delamination factor
200	2000	25.43		1.0433		1.1055

clearance angle of outer cutting edge ( $\alpha_o$ ) was decreased from  $50^\circ$  to  $3^\circ$ . Further, the outer drill tip angle for the 1<sup>#</sup> was 180 degrees and the outer drill tip angle for the 2<sup>#</sup> and 3<sup>#</sup> was 210 degrees. Figure 17 shows the thrust force under the action from the clearance angle of outer cutting edge with candle stick drills, (a) 1<sup>#</sup>, (b) 2<sup>#</sup>, and (c) 3<sup>#</sup>. So, as shown in Fig. 17, in the case of the same cutting thickness, the smaller clearance angle of outer cutting edge, the greater contribution of the clearance angle to the thrust force. That is to say, the smaller clearance angle of outer cutting edge, the larger potential for the push down delamination. But, in fact, the axial  $S_{33}$  stress value, the outside radial lengths of the stress distribution, and the push down delamination along the outside of the hole for the 1<sup>#</sup> were obviously larger than that for the 2<sup>#</sup> and 3<sup>#</sup>. These findings suggested that the outer drill tip angle of 180 degrees had a high negative impact on the push down delamination. At the same time, the axial  $S_{33}$  stress value, the outside radial lengths of the stress distribution, and the push down delamination along the outside of the hole for the 3<sup>#</sup> were greater than that for the 2<sup>#</sup>; this was mainly due to the relatively smaller clearance angle of outer cutting edge for the 3<sup>#</sup>.

#### 4.4 Peel up and push down delamination

As shown in Figs. 11 and 14, the push down delamination was higher than that of the peel up delamination with three candle stick drills. In previous study, it has been also found that the delamination associated with push down was more severe than that associated with peel up [40–42].

### 5 Optimized candle stick drill and verification test

It was clearly seen from the above analysis results of three candle stick drills that the drilling results had a great relationship with the geometric angles of the candle stick drill. For above three candle stick drills, the thrust force was mainly derived from the outer cutting edges. At the same time,

compared to the rake angle of outer cutting edge and the outer drill tip angle, the clearance angle of outer cutting edge had a high impact on the thrust force. So, the thrust force could be greatly reduced by increasing the clearance angle of outer cutting edge. What is more, for the inner cutting edges of the three candle stick drills, the rake and clearance angles of  $0^\circ$  for the inner cutting edge should be avoided in the actual drilling process. For the peel up delamination with above three candle stick drills, the rake angle of the outer cutting edge had a great negative impact on the peel up delamination. At the same time, compared to the outer drill tip angle of 180 degrees, the drill with the outer drill tip angle was greater than 180 degrees could obtain relatively good peel up delamination. So, increasing the rake angle of the outer cutting edge and keeping the outer drill tip angle greater than 180 degrees could reduce the peel up delamination. For the push down delamination with above three candle stick drills, the outer drill tip angle and the clearance angle of the outer cutting edge had a great impact on the push down delamination. Avoiding a 180 degrees outer drill tip angle and increasing the clearance angle of outer cutting edge could reduce the push down delamination.

It was obviously known from the above analysis that optimizing the geometric angles of candle stick drill could reduce thrust force, peel up, and push down delamination. In order to prove this conclusion, this paper optimized the candle stick drill and carried out corresponding verification test. Table 12 and Table 13 show the optimized geometric angles of candle stick drill and corresponding results of verification test. As shown in Table 12 and Table 13, compared with the experimental results shown in Table 8, the optimized candle stick drill achieved relatively excellent drilling results, that is, the optimized candle stick drill achieved relatively lower thrust, peel up, and push down delamination.

### 6 Conclusions

Drilling GFRP composites using candle stick drills and twist drill were carried out. Thrust forces, peel up, and push down

delamination were set as the observable variables. According to the analysis results, it could draw some conclusions.

- Compared to the twist drill, not all candle stick drills could get relatively good drilling results which were relatively lower thrust force, peel up, and push down delamination. For example, in the four drills from the 1<sup>#</sup> to 4<sup>#</sup>, all three candle stick drills generated relatively larger thrust force than the twist drill. What is more, the candle stick drill of 1<sup>#</sup> obtained the lowest peel up delamination, but the worst push down delamination. The candle stick drills of 2<sup>#</sup> and 3<sup>#</sup> produced larger peel up delamination than the twist drill of 4<sup>#</sup>. The candle stick drills of 3<sup>#</sup> got higher push up delamination than the twist drill of 4<sup>#</sup>.
- Drilling results of the candle stick drills had a great relationship with the geometric angles of the candle stick drills. Taking into account thrust force, peel up, and push down delamination, appropriate candle stick drill tip geometry could reduce thrust force and delamination. Under the premise of ensuring the structure strength of the candle stick drills, increasing the rake and clearance angles of the cutting edge could lower thrust force, peel up, and push down delamination. Furthermore, increasing the rake and clearance angles of the inner cutting edge could lower thrust force. Avoiding a 180 degrees outer drill tip angle, that is, keeping the outer drill tip angle greater than 180 degrees, and increasing the rake and clearance angles of the outer cutting edge, could largely reduce thrust force, peel up, and push down delamination.

**Funding information** This project obtained designated funds from the National Natural Science Foundation (No. 51405491, No. 51605331) and the Basic Scientific Research Foundation of Central University (No. 3122017028).

## References

1. HoCheng H, Dharan CKH (1990) Delamination during drilling in composite laminates. *J Eng Ind Trans ASME* 112(3):236–239. <https://doi.org/10.1115/1.2899580>
2. Kavadi BV, Pandey AB, Tadavi MV, Jakharia HC (2014) A review paper on effects of drilling on glass fiber reinforced plastic. *Procedia Technology* 14:457–464. <https://doi.org/10.1016/j.protcy.2014.08.058>
3. Durão LMP, Tavares JMR, De Albuquerque VHC, Marques JFS, Andrade ON (2014) Drilling damage in composite material. *Materials* 7(5):3802–3819. <https://doi.org/10.3390/ma7053802>
4. Giroto F, Dau F, Gutiérrez-Orrantía ME (2017) New analytical model for delamination of CFRP during drilling. *J Mater Process Tech* 240:332–343. <https://doi.org/10.1016/j.jmatprotec.2016.10.007>
5. Palanikumar K, Rubio JC, Abrao A, Esteves A, Davim JP (2008) Statistical analysis of delamination in drilling glass fiber-reinforced plastics (GFRP). *J Reinf Plast Comp* 27(15):1615–1623. <https://doi.org/10.1177/0731684407083012>
6. Latha B, Senthilkumar VS (2009) Fuzzy rule based modeling of drilling parameters for delamination in drilling GFRP composites. *J Reinf Plast Comp* 28(8):951–964. <https://doi.org/10.1177/0731684407087570>
7. Kilickap E (2010) Investigation into the effect of drilling parameters on delamination in drilling GFRP. *J Reinf Plast Comp* 29(23):3498–3503. <https://doi.org/10.1177/0731684410386271>
8. Venkateshwaran N, ElayaPerumal A (2013) Hole quality evaluation of natural fiber composite using image analysis technique. *J Reinf Plast Comp* 32(16):1188–1197. <https://doi.org/10.1177/0731684413486847>
9. Won MS, Dharan CKH (2002) Chisel edge and pilot hole effects in drilling composite laminates. *J Manuf Sci E-T ASME* 124(2):242–247
10. Hocheng H, Tsao CC (2005) The path towards delamination-free drilling of composite materials. *J Mater Process Tech* 167(2):251–264. <https://doi.org/10.1016/j.jmatprotec.2005.06.039>
11. Tsao CC (2007) Taguchi analysis of drilling quality associated with core drill in drilling of composite material. *Int J Adv Manuf Technol* 32(9):877–884. <https://doi.org/10.1007/s00170-006-0414-9>
12. Tsao CC (2008) Thrust force and delamination of core-saw drill during drilling of carbon fiber reinforced plastics (CFRP). *Int J Adv Manuf Technol* 37(1):23–28. <https://doi.org/10.1007/s00170-007-0963-6>
13. Tsao CC (2008) Prediction of thrust force of step drill in drilling composite material by Taguchi method and radial basis function network. *Int J Adv Manuf Technol* 36(1):11–18. <https://doi.org/10.1007/s00170-006-0808-8>
14. Tsao CC, Hocheng H (2004) Taguchi analysis of delamination associated with various drill bits in drilling of composite material. *Int J Mach Tool Manu* 44(10):1085–1090. <https://doi.org/10.1016/j.ijmactools.2004.02.019>
15. Hocheng H, Tsao CC (2001) Delamination models in drilling of composite materials using saw drill and candle-stick drill. *ASME*
16. Tsao CC, Hocheng H (2005) Effect of eccentricity of twist drill and candle stick drill on delamination in drilling composite materials. *Int J Mach Tool Manu* 45(2):125–130. <https://doi.org/10.1016/j.ijmactools.2004.08.001>
17. Palanikumar K (2010) Modeling and analysis of delamination factor and surface roughness in drilling GFRP composites. *Mater Manuf Process* 25(10):1059–1067. <https://doi.org/10.1080/10426910903575830>
18. Palanikumar K, Latha B, Senthilkumar VS, Davim JP (2012) Analysis on drilling of glass fiber-reinforced polymer (GFRP) composites using grey relational analysis. *Mater Manuf Process* 27(3):297–305. <https://doi.org/10.1080/10426914.2011.577865>
19. Palanikumar K, Srinivasan T, Rajagopal K, Latha B (2016) Thrust force analysis in drilling glass fiber reinforced/polypropylene (GFR/PP) composites. *Mater Manuf Process* 31(5):581–586. <https://doi.org/10.1080/10426914.2014.961478>
20. Srinivasan T, Palanikumar K, Rajagopal K, Latha B (2017) Optimization of delamination factor in drilling GFR–polypropylene composites. *Mater Manuf Process* 32(2):226–233. <https://doi.org/10.1080/10426914.2016.1151038>
21. Grilo TJ, Paulo RMF, Silva CRM, Davim JP (2013) Experimental delamination analyses of CFRPs using different drill geometries. *Compos Part B-Eng* 45(1):1344–1350. <https://doi.org/10.1016/j.compositesb.2012.07.057>
22. Wang CD, Qiu KX, Chen M, Cai XJ (2015) Machinability of drilling T700/LT-03A carbon fiber reinforced plastic (CFRP) composite laminates using candle stick drill and multi-facet drill. *Int J Mod Phys B* 29(10n11):1540031
23. Abrão AM, Rubio JC, Faria PE, Davim JP (2008) The effect of cutting tool geometry on thrust force and delamination when drilling glass fibre reinforced plastic composite. *Mater Design* 29(2):508–513. <https://doi.org/10.1016/j.matdes.2007.01.016>
24. Tsao CC (2012) Evaluation of the drilling-induced delamination of compound core-special drills using response surface methodology

- based on the Taguchi method. *Int J Adv Manuf Technol* 62(1–4): 241–247. <https://doi.org/10.1007/s00170-011-3785-5>
25. Durão LMP, Gonçalves DJ, Tavares JMR, de Albuquerque VHC, Vieira AA, Marques AT (2010) Drilling tool geometry evaluation for reinforced composite laminates. *Compos Struct* 92(7):1545–1550. <https://doi.org/10.1016/j.compstruct.2009.10.035>
  26. Tan CL, Azmi AI, Muhammad N (2016) Delamination and surface roughness analyses in drilling hybrid carbon/glass composite. *Mater Manuf Process* 31(10):1366–1376. <https://doi.org/10.1080/10426914.2015.1103864>
  27. Tan CL, Azmi AI (2017) Analytical study of critical thrust force for on-set delamination damage of drilling hybrid carbon/glass composite. *Int J Adv Manuf Technol*:1–13
  28. Chen WC (1997) Some experimental investigations in the drilling of carbon fiber-reinforced plastic (CFRP) composite laminates. *Int J Mach Tool Manu* 37(8):1097–1108. [https://doi.org/10.1016/S0890-6955\(96\)00095-8](https://doi.org/10.1016/S0890-6955(96)00095-8)
  29. Enemuoh EU, El-Gizawy AS, Okafor AC (2001) An approach for development of damage-free drilling of carbon fiber reinforced thermosets. *Int J Mach Tool Manu* 41(12):1795–1814. [https://doi.org/10.1016/S0890-6955\(01\)00035-9](https://doi.org/10.1016/S0890-6955(01)00035-9)
  30. Piquet R, Ferret B, Lachaud F, Swider P (2000) Experimental analysis of drilling damage in thin carbon/epoxy plate using special drills. *Compos Part A-Appl S* 31(10):1107–1115. [https://doi.org/10.1016/S1359-835X\(00\)00069-5](https://doi.org/10.1016/S1359-835X(00)00069-5)
  31. Faraz A, Biermann D, Weinert K (2009) Cutting edge rounding: an innovative tool wear criterion in drilling CFRP composite laminates. *Int J Mach Tool Manu* 49(15):1185–1196. <https://doi.org/10.1016/j.ijmactools.2009.08.002>
  32. Heisel U, Pfeifroth T (2012) Influence of point angle on drill hole quality and machining forces when drilling CFRP. *Procedia CIRP* 1:471–476. <https://doi.org/10.1016/j.procir.2012.04.084>
  33. Raj DS, Karunamoorthy L (2016) Study of the effect of tool wear on hole quality in drilling CFRP to select a suitable drill for multi-criteria hole quality. *Mater Manuf Process* 31(5):587–592. <https://doi.org/10.1080/10426914.2015.1004713>
  34. Hocheng H, Tsao CC (2006) Effects of special drill bits on drilling-induced delamination of composite materials. *Int J Mach Tool Manu* 46(12):1403–1416. <https://doi.org/10.1016/j.ijmactools.2005.10.004>
  35. Chen WC (1997) Some experimental investigations in the drilling of carbon fiber-reinforced plastic (CFRP) composite laminates. *Int J Mach Tools Manuf* 37(8):1097–1108. [https://doi.org/10.1016/S0890-6955\(96\)00095-8](https://doi.org/10.1016/S0890-6955(96)00095-8)
  36. Hibbitt K, Inc S (2011) ABAQUS version:6.11
  37. Isbilir O, Ghassemieh E (2013) Numerical investigation of the effects of drill geometry on drilling induced delamination of carbon fiber reinforced composites. *Compos Struct* 105:126–133. <https://doi.org/10.1016/j.compstruct.2013.04.026>
  38. Hashin Z (1980) Failure criteria for unidirectional fiber composites. *Int J Appl Mech* 47(2):329–334. <https://doi.org/10.1115/1.3153664>
  39. Klinkova O, Rech J, Drapier S, Drapier S, Bergheau JM (2011) Characterization of friction properties at the workmaterial/cutting tool interface during the machining of randomly structured carbon fibers reinforced polymer with carbide tools under dry conditions. *Tribol Int* 44(12):2050–2058. <https://doi.org/10.1016/j.triboint.2011.09.006>
  40. Kalla D, Sheikh-Ahmad J, Twomey J (2010) Prediction of cutting forces in helical end milling fiber reinforced polymers. *Int J Mach Tools Manuf* 50(10):882–891. <https://doi.org/10.1016/j.ijmactools.2010.06.005>
  41. Khashaba UA (2004) Delamination in drilling GFR-thermoset composites. *Compos Struct* 63(3):313–327. [https://doi.org/10.1016/S0263-8223\(03\)00180-6](https://doi.org/10.1016/S0263-8223(03)00180-6)
  42. Khashaba UA, El-Sonbaty IA, Selmy AI, Megahed AA (2010) Machinability analysis in drilling woven GFR/epoxy composites: part I—effect of machining parameters. *Compos Part A-Appl S* 41(3):391–400. <https://doi.org/10.1016/j.compositesa.2009.11.006>